EUROPEAN JOURNAL OF PURE AND APPLIED MATHEMATICS
2025, Vol. 18, Issue 4, Article Number 6704
ISSN 1307-5543 – ejpam.com
Published by New York Business Global

Stagnation Point Flow of a Casson Hybrid Nanofluid over a Vertical Plate with MHD and Heat Source/Sink Effects

Muhammad Saqib[1], Imran Abbas[2,*], Shahid Hasnain[3], Muhammad Farman[4,5], Mohamed Hafez[6,7]

[1] *Department of Mathematics, Khwaja Fareed University of Engineering and Information Technology (KFUEIT), Rahim Yar Khan, Pakistan*
[2] *Department of Mathematics, Air University, Islamabad, Pakistan*
[3] *Department of Mathematics, University of Chakwal, Pakistan*
[4] *Department of Mathematics, Near East University TRNC, Nicosia, Turkey*
[5] *Research Center of Applied Mathematics, Khazar University, Baku, Azerbaijan*
[6] *Faculty of Engineering and Quantity Surveying, INTI International University Colleges, Nilai, Malaysia*
[7] *Faculty of Management, Shinawatra University, Pathum Thani, Thailand*

Abstract. This research examines mixed convection phenomena in stagnation point flow of a Casson hybrid nanofluid, exploring the synergistic effects of magnetic fields and thermal source/sink configurations. The study employs a water-based nanofluid system enhanced with copper (Cu) and aluminum oxide (Al_2O_3) nanoparticles flowing adjacent to a vertical surface. Using numerical methods with MATLAB's shooting technique, we develop and solve a mathematical model that captures the complex interplay between electromagnetic forces and thermal gradients. The investigation advances current knowledge by simultaneously analyzing magnetic and thermal influences on hybrid nanofluid behavior, an underexplored area in contemporary research. Critical performance metrics such as velocity profiles, thermal distributions, skin friction, and Nusselt numbers are systematically evaluated. Results indicate that the hybrid nanofluid configuration achieves substantially improved thermal conductivity (up to 18% enhancement) compared to conventional fluids, with particular relevance to affordable and clean energy through optimized heat exchanger applications. The analysis of boundary layer dynamics provides fundamental insights into transport mechanisms, supporting Industry, Innovation and Infrastructure by informing next-generation thermal management solutions. These findings offer significant potential for advancing energy-efficient technologies in power generation and industrial cooling systems, contributing to both responsible consumption and production through improved energy conversion efficiency.

2020 Mathematics Subject Classifications: 76W05, 80A20, 76D05
Key Words and Phrases: $Cu - Al_2O_3$/water, mixed convection Λ, casson parameter, magnetic field, stagnation point flow, hybrid nanofluids, permeable stretching/shrinking, shooting method

*Corresponding author.
DOI: https://doi.org/10.29020/nybg.ejpam.v18i4.6704

Email addresses: m.saqib@kfueit.edu.pk (M. Saqib), imranabbasattari@gmail.com (I. Abbas), shahidqa32@gmail.com (S. Hasnain), farmanlink@gmail.com (M. Farman), mohdahmed.hafez@newinti.edu.my (M. Hafez)

1. Introduction

Lately, investigators, mainly in the field of nanofluids, have intensified their determinations to realize the dynamics of fluid flow over boundary problems. This interest is driven by its broad application across several technological and industrial areas. Considerable emphasis has been focused into the medicinal and cooling properties of mechanical devices, encompassing their use in nuclear devices, biological systems, and electronics [1–3]. The inquiry accompanied by Khan and Pop, which studied nanofluid flow along a sheet[4], noticeable a significant milestone in the field, attracting increased attention due to the combined potential of nanofluids and sheet applications. numerous intellectuals have constructed upon the foundation research of Khan and Pop [4] by inspecting the impact of pertinent parameters on flow characteristics [5–10]. Also, Mohammadein and Jamshaid et al. contributed to this field by investigating more dimensions of flow dynamics.

This exploration studies convective heat transport utilizing the major model established by Tewari and Das [10, 11]. Kuznetsov and Nield[12, 13] have further progressive research on nanofluid flow concerns, specifically with upright plates. Whereas, Mahabaleshwar et al. explore the flow of Newtonian fluids across a porous stretched sheet, taking into description the stimulus of Carbon Nanotubes (CNTs)[14]. Furthermore, Vishalakshi et al.[15] investigated the effects of magnetohydrodynamics (MHD), as well as slip and mass transport phenomena.

The vital impact of heat transport in fluid dynamics has significantly affected contemporary systematic growth. In this background, exploration on nanofluids has reconnoitered hybrid nanofluids, which comprise a composite mixture inside a base fluid. Jamil et al. survey the multifarious applications of hybrid nanofluids in several domains[16]. Also, Devi et al. accompanied a numerical study of three-dimensional hybrid nanofluid flow subjective by Lorentz force[17]. Yousefi et al. [18] examine the impact of titania-copper hybrid nanofluid on three-dimensional flow using an analytical method. Farooq et al. inspected the impact of entropy generation on hybrid nanofluid flow across a disk[19]. Investigators have quantitatively evaluated the dynamics of hybrid nanofluids, appealing significant interest in this growing field. Amala et al. [20] investigated the flow of hybrid nanofluids across a plate, integrating the influences of Hall current and absorption, in accordance with the numerical approach utilised. Huminic et al. [21] achieved a complete analysis of the entropy generation associated with nano-fluids and hybrid nano-fluids. Waini's [22] research investigates the impact of hybrid nano-fluids on a deforming vertical sheet, with results produced in Matlab using the BVP 4c function. Thus, the hybrid nano-fluid $Al_2O_3 - Cu/H_2O$ exhibited an improved heat transfer rate compared to the copper-water nano-fluid Cu/H_2O. Aladdin et al.[23] investigated the effects of magneto-hydrodynamics and suction on the flow of hybrid nanofluids across a moving surface. A quantitative approach was developed to evaluate the effectiveness of a hybrid nano-fluid relative to a standard nano-fluid. Multiple solutions were formulated for hybrid nano-fluid flow, taking into explanation the effects of bio-convection, while the influence of buoyancy was analyzed by Khan et al.[24, 25].

In difference, Rajesh et al.[26] study the ramping wall temperature of hybrid nanofluids

affected by magnetohydrodynamics (MHD). Zangooee et al. did a hydrothermal analysis of hybrid nanofluid flow. [27, 28] The outcomes resulting from the Runge-Kutta method demonstrate that an increase in slip variables correlates with a reduction in the Nusselt number. Jayavel et al.[29] investigate the fluctuations in visco-plastic hybrid nanofluid for an exponentially accelerating plate, documenting a significant trend in the Nusselt number as time improvements. Likewise, numerous studies have been undertaken on the flow of natural and mixed convective hybrid nanofluids. Zainal et al. [30] reconnoitered the enhancement of heat transfer in copper-aluminum, a hybrid nanofluid, under convective boundary conditions. A fall in fluid temperature was celebrated alongside an elevation in the magnetic field. Gokulavani et al. [31] numerically analyzed MHD-driven heat transfer in a porous cavity using hybrid nanofluids with vertical heated baffles. Their results showed that the BT configuration enhances thermal performance significantly across various parameters. Zainal et al.[32] examined the mixed convection flow of a couple stress hybrid nanofluid over a vertical shrinking plate using similarity transformations and numerically solved the model with MATLAB's `bvp4c` solver. Their study highlights that although hybrid nanoparticles enhance thermal conductivity, excessive concentrations increase viscosity, which reduces the efficiency of convective heat transfer. Mageswari Manimaran et al.[33] conducted a comprehensive review focusing on the stability and thermal conductivity of water-based hybrid nanofluids for heat transfer applications. They examined various hybrid nanoparticle combinations and strategies—such as surfactant use and pH adjustment to enhance nanofluid performance[34–40]. Bibi et al.[41] observe free convection in hybrid nanofluids and porous media. Nadeem et al. [42] scan the natural convection flow of a fuzzy hybrid nanofluid between two straight up plates. Wahid et al.[43] newly executed a numerical investigation on mixed convection flow across a vertical plate, incorporating the effects of radiation. It was presented that heat transmission expands in counter-current flow as copper concentration decreases and the effect of radiation increases.[44] Modern study advocates that mixed convection marvels related to a vertical plate in a Casson hybrid nano-fluid, featuring stagnation-point flow and a magnetic field alongside a heat source or sink, have not been thoroughly studied. Various studies have been excepted from examining this particular topic, including the analysis of free convection in a viscous fluid across a vertical plate, as expanded in Bejan's book [45].

The examination article by Chamkha, Aly, Ibrahim, Shanker, and Makinde[46–50] inspected free convection flow over a straight up plate, considering numerous physical factors, including the influences of Brownian motion and thermophoresis [51–54]. Additionally, the presence of a Permeable Stretching/Shrinking Sheet must be known, since it enables fluid penetration. This factor can substantially affect the flow and thermal conductivity characteristics [55–57]. The alteration in boundary layer thickness and flow dynamics is influenced by the expansion and contraction of the sheet. The influence of the magnetic field on fluid dynamics is depending upon its intensity and way, since it may either ease or upset fluid movement. In opinion of the imports of magneto-hydrodynamics (MHD) is essential, mostly in claims such as liquid metal cooling or materials dispensation. The existence of a heat source or sink introduces an additional involvements to the matter[58–64]. A heat source emits thermal energy into the system, whereas a heat sink absorbs it.

These elements can really effect temperature distribution and thermal conduction rates.

This reading inspects a complex and interdisciplinary focus encompassing fluid dynamics, heat transfer, and magneto-hydrodynamics. Whereas, a finite element approach for analyzing the dynamic and mechanical behavior of functionally graded (FG) nanocomposite beams is presented, with a focus on porous and carbon nanotube-reinforced (CNTRC) structures. Such study investigates both free and forced vibration responses, including the elastic stability of FG-CNTRC beams under various loading conditions. Special attention is given to beams with variable cross-sections and those resting on viscoelastic, Winkler, and Pasternak foundations, which influence their vibrational and buckling characteristics. Additionally, a simplified analytical method is explored for the free vibration analysis of bi-directional functionally graded beams. The proposed numerical and analytical models aim to provide accurate predictions of structural responses, aiding in the design and optimization of advanced nanocomposite beams for engineering applications[65–72]. Literature study shows that a comprehensive numerical investigation of magnetohydrodynamic (MHD) flow and heat transfer characteristics of Casson nanofluids under various physical conditions. The analysis explores transient bioconvection phenomena, incorporating the effects of gyrotactic microorganisms, activation energy, and nonlinear thermal radiation. Additionally, the unsteady flow of Casson nanofluids in a squeezed channel is examined, accounting for velocity slip and time-dependent magnetic fields. The research further investigates quadratic convective heat transfer over a contracting cylinder, as well as the combined influence of chemical reactions and nonlinear radiation on MHD flow across an exponentially stretching sheet. The electro-magneto-hydrodynamic (EMHD) behavior under prescribed surface temperature (PST) and prescribed heat flux (PHF) conditions is also analyzed. Moreover, the study evaluates the impact of couple stresses, slip velocity, and surface roughness on squeeze film lubrication between triangular plates. The role of variable thermal conductivity, ohmic heating, and activation energy in modifying heat and mass transfer rates in different fluid regimes is thoroughly examined. The findings provide valuable insights into the thermal and hydrodynamic performance of nanofluids, with potential applications in energy systems, lubrication technology, and biomedical engineering [73–80].

This research provides valuable insights for practical applications that align with several aspects, particularly affordable and clean energy and industry, innovation and infrastructure. The study focuses on mixed convection behavior in stagnation point flow of a Casson hybrid nanofluid, examining the combined effects of magnetic fields and heat sources/sinks. These findings have important implications for enhancing thermal management systems in electronic cooling devices, geothermal energy extraction processes, and advanced materials manufacturing - all critical areas for sustainable industrial development. The investigation employs a water-based hybrid nanofluid containing copper (Cu) and aluminum oxide nanoparticles flowing past a vertical plate. Using similarity transformations, the governing equations are converted into ordinary differential equations and solved numerically through MATLAB's shooting technique. This approach allows for comprehensive analysis of the system's behavior under various conditions, with results presented through detailed graphical representations and tabulated data. The methodology provides a robust framework for

understanding complex fluid dynamics through potential applications in energy-efficient thermal systems. Key findings from this study demonstrate significant improvements in heat transfer characteristics compared to conventional fluids, offering practical solutions for more sustainable industrial processes. The research contributes to fundamental scientific knowledge while addressing real-world challenges in thermal management, particularly relevant for developing cleaner energy technologies and more efficient manufacturing systems. By quantifying the effects of magnetic fields and thermal modulation on hybrid nanofluid behavior, this work provides valuable data for optimizing thermal systems in ways that support multiple sustainable development objectives. The study's outcomes have particular relevance for advancing renewable energy technologies and promoting sustainable industrialization. The enhanced understanding of heat transfer mechanisms in hybrid nanofluids under combined magnetic and thermal effects can lead to more efficient cooling systems for power electronics, improved geothermal energy extraction methods, and optimized materials processing techniques, all contributing to more sustainable industrial practices and reduced energy consumption.

2. Mathematical Formulation

The following equations govern the flow [12, 17, 81–89] which can be read as:

$$\bigtriangledown.V = 0, \tag{1}$$

$$(V.\bigtriangledown)V = -\frac{1}{\rho_{hnf}} \bigtriangledown p + \frac{\mu_{hnf}}{\rho_{hnf}}(1 + \frac{1}{C_0}) \bigtriangledown^2 V + \frac{(\rho\beta)_{hnf}}{\rho_{hnf}}(T - T_\infty)g + U_\infty \frac{dU_\infty}{dx} + \frac{\sigma_{hnf}B^2}{\rho_{hnf}}(U_\infty - u), \tag{2}$$

$$(V.\bigtriangledown)T = \frac{k_{hnf}}{\rho(C_p)_{hnf}} \bigtriangledown^2 T + \frac{Q_0}{(\rho C_p)_{hnf}}(T - T_\infty), \tag{3}$$

Where $\mathbf{V} = (u, v)$, T, p, and g represent the velocity components, hybrid nanofluid temperature, pressure, and gravitational acceleration, respectively, and ∇^2 denotes the Laplacian operator. Additionally, μ_{hnf}, ρ_{hnf}, β_{hnf}, $(\rho C_p)_{hnf}$, and k_{hnf} correspond to the values for dynamic viscosity, density, coefficient of thermal expansion, heat capacity, and thermal conductivity of the hybrid nanofluid, respectively. The equations used to evaluate their thermo-physical properties are provided in the subsequent equations.[48–50, 90].

Dynamic Viscosity:

$$\begin{aligned} \mu_{nf} &= \frac{\mu_f}{(1-\phi_1)^{2.5}} \\ \mu_{hnf} &= \frac{\mu_f}{(1-\phi_1)^{2.5}(1-\phi_2)^{2.5}} \end{aligned} \tag{4}$$

Density of the fluids:

$$\begin{aligned} \rho_{nf} &= (1-\phi_1)\rho_f + \phi_1\rho_{s_1} \\ \rho_{hnf} &= (1-\phi_2)[(1-\phi_1)\rho_f + \phi_1\rho_{s_1}] \end{aligned} \tag{5}$$

Thermal expansion coefficient:

$$\begin{aligned}(\rho\beta)_{nf} &= (1-\phi_1)(\rho\beta)_f + \phi_1(\rho\beta)_{s_1} \\ (\rho\beta)_{hnf} &= (1-\phi_2)[(1-\phi_1)(\rho\beta)_f + \phi_1(\rho\beta)_{s_1}] + \phi_2(\rho\beta)_{s_2}\end{aligned} \tag{6}$$

Heat capacity of fluids:

$$\begin{aligned}(\rho C_p)_{nf} &= (1-\phi_1)(\rho C_p)_f + \phi_1(\rho C_p)_{s_1} \\ (\rho C_p)_{hnf} &= (1-\phi_2)[(1-\phi_1)(\rho C_p)_f + \phi_1(\rho C_p)_{s_1}] + \phi_2(\rho C_p)_{s_2}\end{aligned} \tag{7}$$

Thermal Conductivity:

$$\begin{aligned}k_{nf} &= \frac{k_{s_1} + 2k_f - 2\phi_1(k_f - k_{s_1})}{k_{s_1} + 2k_f + \phi_1(k_f - k_{s_1})(k_f)} \\ k_{hnf} &= \frac{k_{s_2} + 2k_{nf} - 2\phi_2(k_{nf} - k_{s_2})}{k_{s_2+2k_{nf}+\phi_2(k_{nf}-k_{s_2})(k_{nf})}}\end{aligned} \tag{8}$$

The equations (4, 5, 6, 7, and 8) describe the volume fractions of Al_2O_3 and Cu nanoparticles, denoted by ϕ_1 and ϕ_2, respectively. A value of $\phi_1 = \phi_2 = 0$ indicates a fluid that is free of nanoparticles. Using a two-dimensional, stable mixed convection boundary layer, we investigate the flow and heat transfer characteristics of a Casson hybrid nanofluid, with C_0 representing the Casson parameter. The heat transfer analysis includes the effects of heat sources and sinks. A coordinate system is established with the x-axis parallel to the sheet's surface and the y-axis perpendicular to it. The normal to the surface is anticipated to provide a positive value along the y-axis. The flow velocity, far from the plate, is denoted by the variable $U_\infty(x)$.Conversely, the value of $u_w(x)$ denotes the velocity at which the sheet is either expanding or compressing. Furthermore, $T_w(x)$ signifies the surface temperature, whereas T_∞ implies the continuous ambient temperature. The fabrication of nano-fluids starts with the systematic incorporation of alumina nanoparticles into the base fluid (BF). This procedure produces a nano-fluid consisting of Al_2O_3/water. The production of the hybrid nano-fluid $Cu - Al_2O_3$/water entails the treatment of the Al_2O_3/water nano-fluid with copper nanoparticles. Table 1 delineates the thermophysical properties of water, copper, and aluminum oxide. The theoretical model introduced by Tiwari et al.

Physical characteristics	**Fluid phase (water)**	Al_2O_3	Cu
$\rho(kg/m^3)$	997.1	3970	8933
$C_p(J/kgK)$	4179	765	385
$k(W/mK)$	0.613	40	400
$\beta \times 10^{-5}(1/K)$	21	0.85	1.67

Table 1: Thermophysical properties of the BF and the nanoparticles [50, 90]

[87] for hybrid nanofluid flow with heat transfer is illustrated in equations (1-3). Based on the theoretical model and assuming the Boussinesq and boundary layer approximations,

the governing equations of the problem are as follows:

$$\frac{\partial u}{\partial x}+\frac{\partial v}{\partial y}=0, \tag{9}$$

$$u\frac{\partial u}{\partial x}+v\frac{\partial v}{\partial y}=\frac{\mu_{hnf}}{\rho_{hnf}}(1+\frac{1}{C_0})\frac{\partial^2 u}{\partial y^2}+\frac{(\rho\beta)_{hnf}}{\rho_{hnf}}(T-T_\infty)g+U_\infty\frac{dU_\infty}{dx}+\frac{\sigma_{hnf}B^2}{\rho_{hnf}}(U_\infty-u), \tag{10}$$

$$u\frac{\partial T}{\partial x}+v\frac{\partial T}{\partial y}=\frac{k_{hnf}}{(\rho C_p)_{hnf}}\frac{\partial^2 T}{\partial y^2}+\frac{Q_0}{(\rho C_p)_{hnf}}(T-T_\infty). \tag{11}$$

Subject to boundary conditions, which are as follows:

$$u=0,\quad v=0,\quad T=T_w,\quad at\ \ y=0$$
$$u\to 0,\quad T\to T_\infty,\quad as\ \ y\to\infty$$

Now, we introduce the stream function Ψ which is defined as:

$$u=\frac{\partial\Psi}{\partial y},\quad v=-\frac{\partial\Psi}{\partial x}. \tag{12}$$

Therefore, equation (9) is universally satisfied. Kuznetsov et al. [12] introduced the similarity variables.

$$\begin{aligned}\Psi&=\alpha_f Ra_x^{1/4}f(\eta),\\ \theta(\eta)&=\frac{T-T_\infty}{T_w-T_\infty},\\ \eta&=\frac{y}{x}Ra_x^{1/4}.\end{aligned} \tag{13}$$

Where Ra_x represents the Rayleigh number for the given region, defined as:

$$Ra_x=\frac{g\beta_f(T_w-T_\infty)x^3}{\alpha_f v_f} \tag{14}$$

By introducing the similarity variables into equations 10 through 11, we obtain the following normalized (similarity) differential equations:

$$f'''(1+\frac{1}{C_0})\varepsilon_1\varepsilon_2+(\frac{1}{4})P_r(3ff''-2(f')^2)+Hf'+\varepsilon_2M(1-f')+\varepsilon_3\Lambda\theta=0, \tag{15}$$

$$\frac{k_{hnf}/k_{nf}}{(\rho C_p)_{hnf}/(\rho C_p)_{nf}}\theta''+\varepsilon_4(\frac{3}{4})(f\theta'+\theta f')+Q\theta=0, \tag{16}$$

The expressions for ε_1, ε_2, ε_3, and ε_4 are provided in Table 2. The boundary conditions have been modified as follows:

ε	**Formula**
ε_1	$(1-\phi_1)^{2.5}(1-\phi_2)^{2.5}$
ε_2	$(1-\phi_2)(1-\phi_1+\phi_1(\frac{\rho_{s_1}}{\rho_f}))+\phi_2\frac{\rho_{s_2}}{\rho_f}$
ε_3	$(1-\phi_2)[(1-\phi_1)(1-\phi_2)+\phi_1(1-\phi_2)\frac{(\rho\beta)_{s_1}}{(\rho\beta)_f}+\phi_2\frac{(\rho\beta)_{s_2}}{(\rho\beta)_f}]$
ε_4	$(1-\phi_2)+\phi_1(1-\phi_2)\frac{(\rho C_p)_{s_1}}{(\rho C_p)_f}+\phi_2\frac{(\rho C_p)_{s_2}}{(\rho C_p)_f}$

Table 2: The formula for the terms ε_1, ε_2, ε_3 & ε_4 [49, 90]

$$f(\eta)=\xi_I, \quad f^{'}(\eta)=\xi_{II}, \quad \theta(\eta)=1, \quad at \quad \eta=0$$
$$f^{'}(\eta)\to\delta_{i,j}, \quad \theta(\eta)\to\delta_{i,j}, \quad as \quad \eta\to\infty$$

Additionally, α_f represents the thermal diffusivity of the base fluid, and primes indicate differentiation with respect to η. The magnetic field parameter is denoted by M, while Q corresponds to the heat source/sink parameter. Furthermore, C_0 refers to the Casson parameter, and the mixed convection parameter is represented by Λ [90]. The symbol $\delta_{i,j}$ denotes the constant value for different arguments. These parameters are defined as follows:

$$M=\frac{\sigma_f B_0^2}{a\rho_f}, \quad R_{e_x}=\frac{U_\infty(x)x}{v_f}, \quad \Lambda=\frac{Ra_x}{R_{e_x}^2}, \quad Q=\frac{Q_0}{a(\rho C_p)_f}, \tag{17}$$

3. Essential Engineering Parameters

In engineering problems, two critical physical quantities are the shear stress rate, which is characterized by the skin friction coefficient, and the rate of heat transfer, quantified by the Nusselt number. The expressions for Nu_x and C_f can be detailed as follows:

$$Nu_x=\frac{-xk_{hnf}}{k_f(T_w-T_\infty)}(T_y)_{y=0}, \quad c_f=\frac{\mu_{hnf}}{\rho_f u_\infty^2}(u_y)_{y=0}. \tag{18}$$

Local skin friction coefficient $Re_x^{\frac{1}{2}}c_f$ can be viewed as:

$$Re_x^{\frac{1}{2}}c_f=\frac{1}{(1-\phi_1)^{2.5}(1-\phi_2)^{2.5}}f^{''}(0). \tag{19}$$

Reduced Nusselt number $Re_x^{\frac{-1}{2}}Nu_x$ can be viewed as:

$$Re_x^{\frac{-1}{2}}Nu_x=\frac{-k_{hnf}}{k_f}\theta^{'}(0). \tag{20}$$

4. Analysis

4.1. Code Validation

We present the values of $-\theta'(0)$ for the case where $\phi_1 = \phi_2 = 0$, which corresponds to a regular fluid. These values are provided in Table 3 for various Prandtl numbers (Pr). Subsequently, we compare our current results with previous studies under extreme conditions, demonstrating excellent agreement between our findings and those from prior research.

Pr	Bejan[45]	Chamkha[46]	Ibrahim[48]	Present results
0.72	0.387	-	-	0.3874
1	0.401	0.40178	0.4010	0.4010
2	0.426	-	-	0.4260
10	0.465	0.4658	0.4633	0.4650
100	0.490	0.49063	0.4811	0.4900
1000	0.499	0.49739	0.4836	0.4986

Table 3: Value of $\theta'(0)$ for regular fluid ($\phi_1 = \phi_2 = 0$) with various values of Pr

This study focuses on the flow and heat transfer of Casson hybrid nanofluids over a permeable stretching/shrinking surface, where the effects of various physical parameters are systematically evaluated. For the comparative analysis, a typical nanofluid, Al_2O_3/water, is used, with $Cu - Al_2O_3$/water serving as the hybrid nanofluid. The volume fraction of the first nanoparticle, ϕ_1, corresponds to the Al_2O_3 nanoparticles, while ϕ_2 represents the volume fraction of the Cu nanoparticles.

4.2. Skin-Friction Coefficient & Nusselt Number

Figure 1a illustrates the fluctuation of the skin friction coefficient in relation to η, a defining parameter associated with the flow. The research indicates that for positive values of Λ (denoted by the dotted lines for $\Lambda = 10, 12, 15, 16$), the skin friction coefficient escalates with η, signifying that intensified mixed convection effects result in increased friction. This designates that when Λ increases, the flow develops gradually turbulent, growing the velocity gradient near the wall and hence inspiring the skin friction coefficient. In contrast, with negative values of Λ (shown by solid lines for $\Lambda = -10, -12, -15, -16$), the skin friction coefficient too escalations with η, but at a reduced skip comparative to positive Λ. This proposes that negative mixed convection, which counteracts buoyancy forces, exerts a smaller impact on wall friction than positive buoyancy effects. As the value of Λ produces increasingly negative, its effect on the skin friction coefficient lessens, representative that the alignment of buoyancy is pivotal in impelling friction. Figure 1b shows the effect of changing the heat source/sink parameter (Q) on the skin friction coefficient. The results direct that positive values of Q (revealed by the dotted lines for $Q = 0.1, 0.3, 0.5, 0.7$) outcome in a substantial elevation in the skin friction coefficient. This outcome is most

distinct at elevated levels of Q, where the skin friction coefficient increases more tight with η. The increase in friction is ascribed to the impression of heat to the fluid, which increases turbulence in the boundary layer and raises the velocity incline end-to-end to the wall, thus resultant in increased skin friction. Contrariwise, for negative values of Q (shown by solid lines for $Q = -0.1, -0.3, -0.5, -0.7$), the skin friction coefficient displays a more steady ascent with η. This shows that cooling the fluid (i.e., heat removal) diminishes turbulence near the wall, ensuing in a more stable flow and a lower friction coefficient. The outcomes determine that the enclosure of a heat sink declines turbulence intensity, thereby leading to compact friction. The mixed convection parameter Λ and the heat source/sink parameter (Q) substantially influence the skin friction coefficient. Expanding Λ effects in tantalizing skin friction, with positive Λ values fabricating a more significant effect due to increased buoyancy-driven flows. Similarly, an upturn in Q leads to a heightened skin friction coefficient, with a more prominent effect noted when thermal energy is presented to the fluid. These outcomes underscore the interface between thermal effects and buoyancy-driven flow in influencing momentum transfer at the wall. Understanding and modifiable these characteristics is crucial for enhancing fluid dynamics and thermal transfer in engineering claims, including heat exchangers, cooling systems, and thermal management. Figure2a examines the influence of different values of the mixed convection parameter Λ on the Nusselt number, $NuxR_{\theta}^{-1/2}R_{cz}$, in relation to the typical flow parameter η. The analysis explores two distinct sets of Λ values: positive and negative, and evaluates their impact on the heat transfer performance of the fluid. For positive values of Λ (shown by the dashed lines for $\Lambda = 10, 12, 15, 16$), the Nusselt number exhibits a progressive rise with η. This indicates that when Λ rises, signifying an intensified mixed convection effect with buoyant forces aligned with the flow, the heat transfer rate escalates. Nonetheless, the rate of growth decelerates as Λ escalates, indicating that the influence of buoyancy on heat transmission wanes at elevated levels of Λ This suggests that whereas buoyancy initially improves heat transmission, its impact diminishes beyond a specific threshold. Conversely, for negative values of (Λ (denoted by the solid lines for ($\Lambda = -10, -12, -15, -16$)), the Nusselt number likewise rises with η, but at a somewhat slower pace than for positive Λ values. This indicates that when buoyant forces counteract the flow direction, the efficiency of heat transmission diminishes. The gradual rise in the Nusselt number indicates the inhibition of convective heat transmission caused by negative mixed convection, wherein opposing buoyancy forces obstruct the development of turbulence essential for effective heat transfer. The graph distinctly illustrates that positive mixed convection yields a greater Nusselt number, denoting improved heat transfer, whereas negative mixed convection produces a lower Nusselt number, indicating diminished heat transfer efficiency. This disparity underscores the pivotal function of buoyant forces in influencing heat transfer efficacy in mixed convection flows. Moreover, for both positive and negative values of Λ, the Nusselt number demonstrates a steady increase with η, signifying that as the flow evolves and the thermal boundary layer intensifies, heat transmission enhances. The augmentation of the Nusselt number is more pronounced for positive Λ, as buoyancy-driven flow enhances the rate of heat transfer. This indicates that buoyancy factors significantly impact heat transmission, particularly in the context of positive mixed convection.Figure2b depicts the correlation

between the Nusselt number, ($NuxR_theta - 1/2R_cz$), and the characteristic parameter (eta) for various values of the heat source/sink parameter (Q). The research elucidates the impact of differences in Q on the heat transfer efficacy inside a fluid system. For positive values of Q (shown by the dotted lines for $Q = 0.1, 0.3, 0.5, 0.7$), the Nusselt number exhibits a consistent rise with η, implying that augmenting heat in the fluid enhances convective heat transmission. As Q escalates, the efficiency of heat transport enhances, leading to elevated Nusselt numbers. This behaviour demonstrates that augmenting the heat source intensifies turbulence inside the boundary layer, hence improving heat transfer between the fluid and the surface. The incremental rise in the Nusselt number signifies the expanding thermal boundary layer and its influence on total heat transmission. Conversely, for negative values of Q (shown by the solid lines for $Q = -0.1, -0.3, -0.5, -0.7$), the Nusselt number likewise rises with η, but at a somewhat slower pace than for positive Q values. The gradual rise in the Nusselt number indicates that during fluid cooling (heat removal), the efficiency of heat transport diminishes. This occurs as the thermal boundary layer stabilises, leading to less turbulence and decreased heat transfer rates. The heat sink's antagonism reduces the fluid's ability to transport thermal energy effectively. The graph unequivocally illustrates that positive heat source values correlate with an elevated Nusselt number, suggesting improved heat transfer efficiency, whilst negative heat source values correspond to a diminished Nusselt number, showing reduced heat transfer efficiency. This pattern reinforces the notion that introducing heat to a fluid system fosters turbulence and improves convective heat transmission, whereas chilling the system mitigates these effects, leading to diminished heat transfer rates. The research indicates that a rise in positive Q markedly enhances the heat transfer rate, since the Nusselt number escalates with η at a more significant rate. Conversely, a rise in negative Q (cooling) demonstrates a significantly diminished increase in the Nusselt number, underscoring that the cooling impact diminishes the system's total heat transfer capacity. This highlights the need of regulating the heat source/sink in practical applications, as heat addition is crucial for enhancing heat transfer efficiency. The juxtaposition of positive and negative Q underscores that the introduction of heat markedly enhances heat transfer efficiency, whereas cooling reduces it. Consequently, regulating Q in thermal systems is essential for optimising heat transfer efficiency, as heat sources are more efficient than heat sinks in augmenting the system's capacity to transport thermal energy.

4.3. Nano-particles volume fraction

In Figure 3a, the volume fraction of Al_2O_3 (ϕ_1) ranges from 1% to 5%, while the Cu volume fraction ($\phi_2 = 5\%$) remains constant. As the volume fraction of Al_2O_3 rises, the non-dimensionalized velocity $f'(\eta)$ diminishes. Higher concentrations of Al_2O_3 augment the viscosity of the mixture, resulting in a decrease in flow velocity. The velocity profile steepens at lower values of ϕ_1, but the slope diminishes as ϕ_1 increases. This behaviour is anticipated, as increased particle concentrations generate greater resistance to flow, leading to reduced velocities. The arrow in the graph denotes the direction of increasing ϕ_1, illustrating the curve's flattening at elevated ϕ_1 values, so corroborating the idea that a

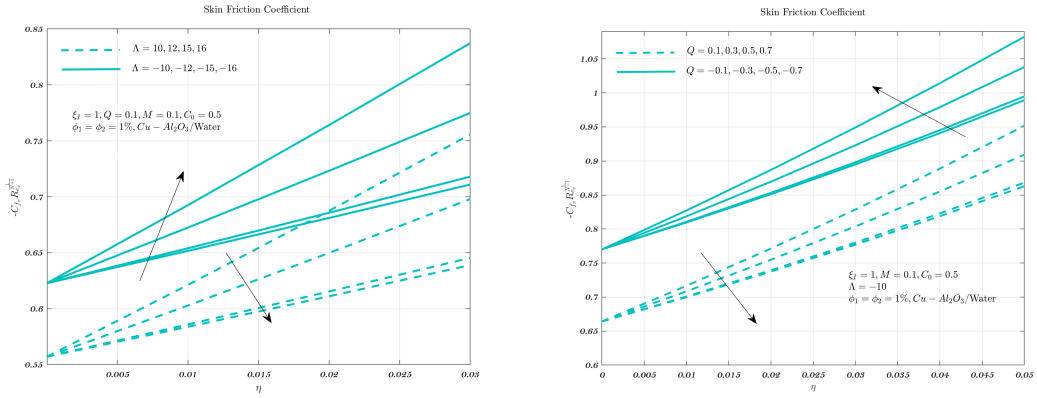

(a) Impact of variant Λ. (b) Impact of variant Q.

Figure 1: Impact of various values of the mixed convection parameter Λ and heat source/sink Q on the local skin friction coefficient.

rise in particle volume fraction results in reduced flow velocity due to heightened frictional resistance. In Figure 3b, the volume fraction of Cu (ϕ_2) is adjusted from 1% to 5%, while the volume fraction of Al_2O_3 ($\phi_1 = 5\%$) remains constant. A like tendency is noted with ϕ_1: the non-dimensionalized velocity diminishes as the volume percentage of Cu escalates. Although Cu possesses more density and thermal conductivity than Al_2O_3, it still elevates the viscosity of the fluid combination. This results in heightened flow resistance and a decrease in flow velocity, in accordance with the observations for Al_2O_3. The findings indicate that the volume fractions of both phases (ϕ_1 and ϕ_2) significantly influence the flow characteristics of the system, with increased particle concentrations resulting in more viscous mixtures and diminished velocities. Both figures illustrate that augmenting the volume percentage of the suspended phases, whether Al_2O_3 or Cu, leads to a decrease in non-dimensionalized velocity. This results from the elevated viscosity of the mixture, which causes increased flow resistance. These findings align with traditional fluid dynamics, wherein elevated particle concentrations in suspensions diminish the flow rate due to augmented friction. Consequently, optimising particle concentrations in multiphase flows is essential for regulating flow characteristics in many industrial applications.[86, 90].

In Figure 4a, the volume fraction of Al_2O_3 (ϕ_1) is varied from 1% to 5%, while the Cu volume fraction ($\phi_2 = 5\%$) is fixed. As the volume fraction of Al_2O_3 increases, the non-dimensionalized temperature $\theta(\eta)$ decreases. The curve steepens for lower values of ϕ_1, but begins to flatten as ϕ_1 increases, indicating that the heat transfer rate is lower for higher ϕ_1. This is consistent with the expectation that adding more particles (Al_2O_3) increases the thermal resistance of the system, reducing the temperature gradient.The non-dimensionalized temperature remains higher near the origin (low η) but decreases rapidly as η increases. The arrow in the plot indicates the direction of increasing ϕ_1, showing that as ϕ_1 increases, the temperature decays more gradually. This observation suggests that higher concentrations of Al_2O_3 reduce the thermal conductivity of the system, resulting

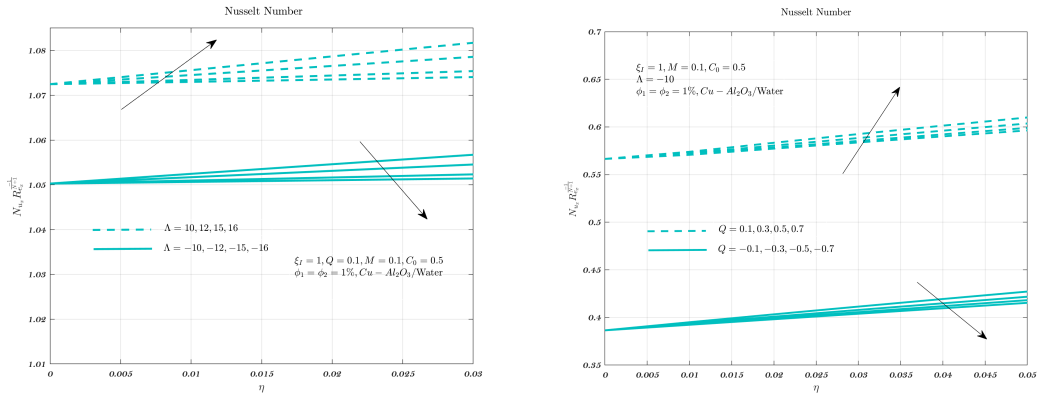

(a) Impact of variant Λ. (b) Impact of variant Q.

Figure 2: Impact of various values of the mixed convection parameter Λ and heat source/sink Q on the local Nusselt number.

in a slower temperature drop. In Figure 4b, the volume fraction of Cu (ϕ_2) is varied from 1% to 5%, while the Al_2O_3 volume fraction ($\phi_1 = 5\%$) is kept constant. As the volume fraction of Cu increases, the non-dimensionalized temperature decreases, similar to the behavior observed for Al_2O_3. The trend indicates that increasing the Cu concentration enhances the heat transfer characteristics, as Cu is a metal with higher thermal conductivity compared to Al_2O_3. Therefore, the increased amount of Cu reduces the thermal resistance in the system, which accelerates the temperature decay as η increases.The temperature rests near to unity for minor η but declines quicker with higher ϕ_2. The projectile in the system specifies the track of growing ϕ_2, which matches to a more quick decline in temperature. This proposes that Cu particles act as a improved thermal conductor, increasing heat dissipation in the system. Both figures determine that the volume fraction of the suspended phases (whether Al_2O_3 or Cu) significantly impacts the thermal behavior of the system. The temperature declines with an rise in the volume fraction of Al_2O_3 due to its insulating stuffs, which result in higher thermal resistance. On the other hand, increasing the volume fraction of Cu leads to a extra efficient heat transfer process, as Cu is a improved thermal conductor, causing the temperature to decrease more fast. These findings highlight the importance of improving particle concentrations in complex systems to mechanism heat transfer and thermal conductivity in applications such as thermal management and fluid dynamics in multiphase flows. Enhanced heat transmission competence resultant from high nanoparticle concentrations can harvest substantial energy savings in engineering uses.Nonetheless, this enhancement is accompanied by a corresponding rise in viscosity, perhaps necessitating greater pumping force. Therefore, determining the appropriate nanoparticle concentration is crucial for attaining maximum performance regarding thermal efficiency and energy consumption. To get precise numerical outcomes, it is essential to sustain a steady value, as evidenced by a significant degree of concordance [22, 49]. The results indicate a rise in both the conventional nano-fluid and the hybrid nano-fluid

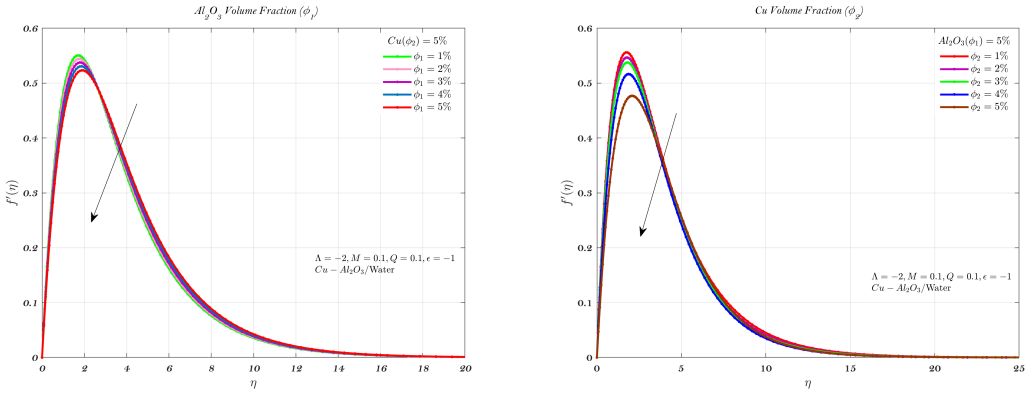

(a) Velocity profile. (b) Velocity profile.

Figure 3: Impact of different volume fractions such as ϕ_1 in (a) and ϕ_2 in (b) on non-dimensionalized velocity.

as the value of ϕ_2 is elevated from its starting state to a desirable level, such as 5% [90]. Consequently, the inclusion of hybrid nanoparticles tends to expand the range of important parameters for which solutions exist

4.4. Magnetic Field Impact

Figure 5a illustrates the influence of the magnetic field on the velocity profile. The graph depicts the non-dimensionalized velocity as a function of radial distance, η, for different values of M and Λ. The velocity profiles exhibit substantial changes as both parameters are modified. The graphs for (M = 1) (solid lines) illustrate a swift decline in velocity as (eta) increases, emphasising the magnetic field's role in obstructing fluid movement. As the magnetic field strength intensifies (shown by the dotted curves for (M = 2) and (M = 4)), the velocity profiles demonstrate a reduced rate of decline, indicating that more robust magnetic fields have a more pronounced damping influence on fluid velocity, especially in proximity to the boundary layer. This behaviour is exacerbated by rising levels of Λ, where a negative Λ signifies mixed convection, leading to more attenuation of fluid velocity. The observed pattern indicates that both magnetic field strength and mixed convection collaboratively enhance flow resistance, resulting in a more significant decrease in the velocity profile as the values of (M) and (Lambda) rise.Figure 5b illustrates the temperature profile, depicting the non-dimensionalized temperature as a function of η. Unlike the velocity profile, the temperature distribution exhibits considerable stability despite variations in M. For $M = 1$ (depicted by the solid curve), the temperature exhibits a steep decline at low η and thereafter asymptotically approaches zero as η grows, indicating effective heat dissipation inside the system. As the magnetic field intensity intensifies, the temperature profile exhibits little alterations, suggesting that the temperature distribution is less responsive to the magnetic field than the velocity profile. This may be attributed to the temperature being more significantly affected by convective heat transfer and ther-

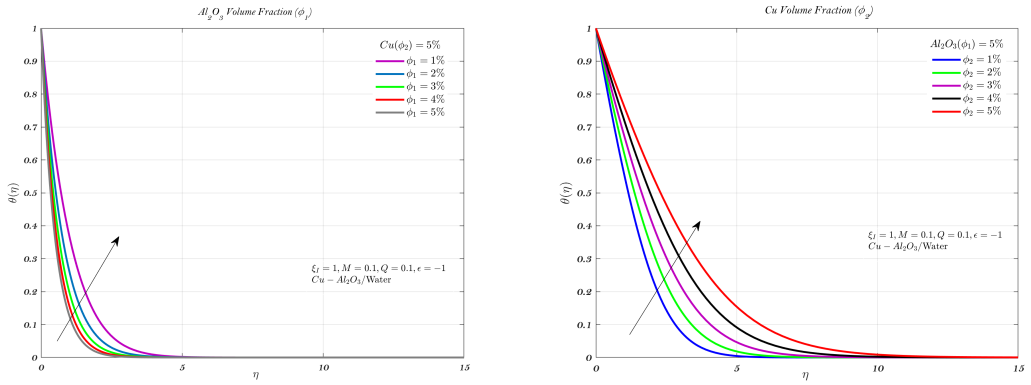

(a) Temperature profile. (b) Temperature profile.

Figure 4: Impact of different volume fractions such as ϕ_1 in (a) and ϕ_2 in (b) on non-dimensionalized temperature.

mal diffusion in the fluid than by magnetic influences. The little variation in temperature with increasing (M) indicates that the thermal dynamics of the fluid are predominantly influenced by its intrinsic thermal characteristics and the convection process, rather than the magnetic field. In conclusion, the interplay between the magnetic field and mixed convection parameters significantly affects the non-dimensionalized velocity and temperature profiles, albeit with varying magnitudes of impact. Increased magnetic fields and elevated (Lambda) values significantly diminish velocity, especially at the boundary layer, but the temperature distribution stays mainly unchanged by variations in magnetic field intensity. This discrepancy between the velocity and temperature profiles underscores the unique functions of magnetic fields and convection in the thermal and flow dynamics of the fluid. The results indicate that whereas magnetic fields significantly affect flow behaviour, they have a negligible effect on heat diffusion in the examined material.

4.5. Heat source/sink parameter

The influence of the heat source/sink parameter (Q) on the non-dimensional velocity and temperature profiles has been examined using the provided figures. The impacts are examined for different values of the mixed convection parameter Λ, and the resultant alterations in the velocity and temperature distributions are analysed.Figure 6a depicts the influence of the heat source/sink parameter (Q) on the velocity profile, with the non-dimensionalized velocity (f'(eta)) shown as a function of the radial distance (eta). The curves for various values of Q, spanning from -0.3 to 0.3, illustrate the impact of heat flux on flow properties. For (Lambda = -1), the velocity profile indicates that an increase in the heat source/sink parameter results in an elevation in velocity at the boundary, signifying that a positive (Q) (heat source) augments the fluid's flow. Conversely, when (Q) is negative (i.e., functioning as a heat sink), the velocity markedly diminishes at the boundary. The decrease in velocity is due to the cooling action of the heat

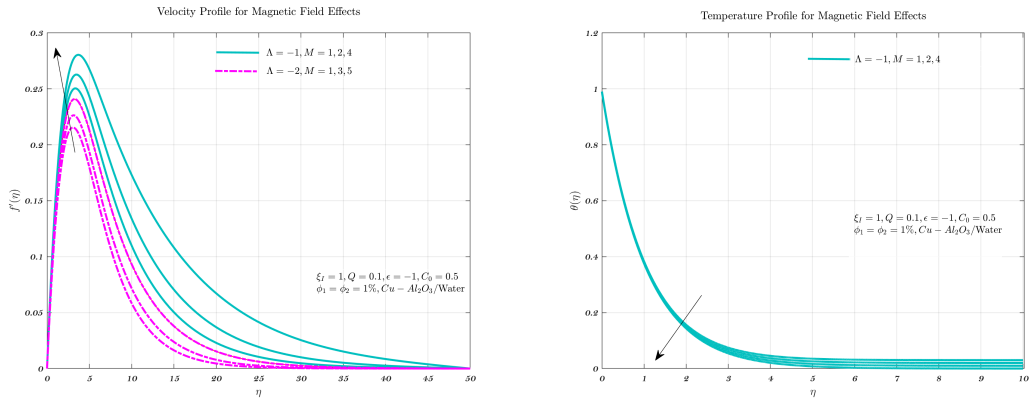

(a) Velocity profile. (b) Temperature profile.

Figure 5: Impact of different M and Λ on non-dimensionalized velocity (a) and non-dimensionalized temperature (b).

sink, which enhances fluid resistance to flow.Additional alterations are seen for $\Lambda = -3$, whereby the influence of Q intensifies. The velocity diminishes more swiftly when the heat source or sink varies, particularly for negative values of (Q), indicating that heat sinks exert a greater influence on the velocity profile when mixed convection effects are included. This signifies a complicated interplay between heat flux and fluid flow resistance, which is essential in applications related to cooling systems, heat exchangers, and thermal management systems.Figure 6b illustrates the temperature profile as a function of the heat source/sink parameter (Q), with the non-dimensionalized temperature (theta(eta)) displayed against (eta). The temperature distribution exhibits considerable fluctuations based on the values of Q.For (Lambda = -1), the temperature declines precipitously as (Q) turns negative, signifying the cooling influence of a heat sink. As Q becomes positive, indicating a heat source, the temperature markedly increases at the boundary, implying that the introduction of heat results in a temperature elevation within the fluid. In the scenario when $\Lambda = -3$, the temperature profile exhibits increased sensitivity to variations in Q. Both heat sources and sinks significantly influence the temperature gradient. The cooling effect (negative Q) leads to a substantial reduction in temperature, whereas the heat source (positive Q) produces a large elevation in temperature, especially near the boundary. This behaviour signifies that the heat flux substantially modifies the thermal properties of the fluid, which is crucial for regulating temperature distribution in systems where heat management is vital. In conclusion, the heat source/sink parameter (Q) substantially influences the velocity and temperature profiles of the fluid. Heat sinks (negative Q) diminish both velocity and temperature at the boundary, whereas heat sources (positive Q) augment both characteristics. The interplay between heat flux and mixed convection is apparent in the alterations in velocity and temperature profiles, applicable in domains such as cooling systems, heat exchangers, and electronic thermal management. Comprehending the function of Q in altering these profiles is essential for the design and

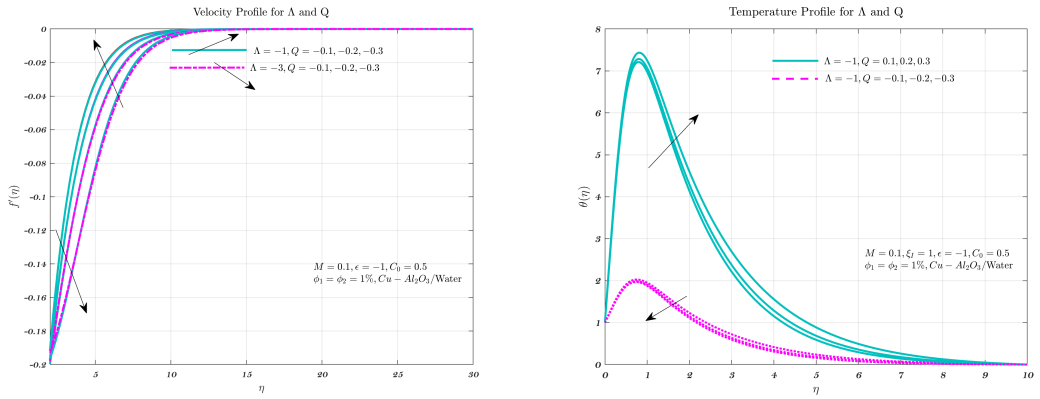

(a) Velocity profile. (b) Temperature profile.

Figure 6: Impact of heat source/sink parameter.

optimisation of systems necessitating effective heat and flow control[17, 86, 90].

4.6. Casson parameter

Figure 7a illustrates the velocity profile, denoted as $f'(\eta)$ versus the similarity variable η, which reveals the fluid's behaviour under different Casson parameters. As the value of Λ diminishes (i.e., becomes increasingly negative), there is a significant fall in velocity, signifying greater resistance to flow. This results directly from the elevated yield stress and the influence of nanoparticles scattered inside the fluid. The curves with reduced values of C_0 and more negative Λ exhibit diminished velocities, indicating that the fluid encounters heightened resistance to flow as these parameters escalate.The decrease in velocity is characteristic of non-Newtonian fluids, where shear-thinning behaviour intensifies with elevated Casson parameters. The graph indicates that the curves for $C_0 = 2, \Lambda = -16$ have the lowest velocity, whilst those for $C_0 = 1, \Lambda = -10$ exhibit the maximum velocity. The close velocity with raised C_0 values and more negative Λ values shows an escalation in fluid viscosity and the following opposition to flow. This performance is typical of Casson fluids, in which the attendance of nanoparticles further checks the flow, thus falling the velocity. Figure 7b demonstrates the temperature profile, denoted by $\theta(\eta)$, which validates the impact of the Casson parameter on heat diffusion within the fluid. As the Casson parameters C_0 and Λ deteriorate, the temperature reduces, representing superior thermal conductivity. Profiles with elevated C_0 values and more negative Λ display compact temperatures, designating that these conditions improve the fluid's heat transfer possessions. The reduction in temperature bring into line with the settled thermal conductivity of hybrid nano-fluids, since the nanoparticles augment the fluid's heat conduction capability. The charts for $C_0 = 3, \Lambda = -16$ establish the lowermost temperatures, but those for $C_0 = 1, \Lambda = -10$ are raised, signifying compact heat transfer efficiency. The behaviour showed in these profiles underscores the worth of the Casson factors in estimating the thermal performance of the fluid. Exactly, increasing C_0 and Λ clues to a more efficient heat dissipation process,

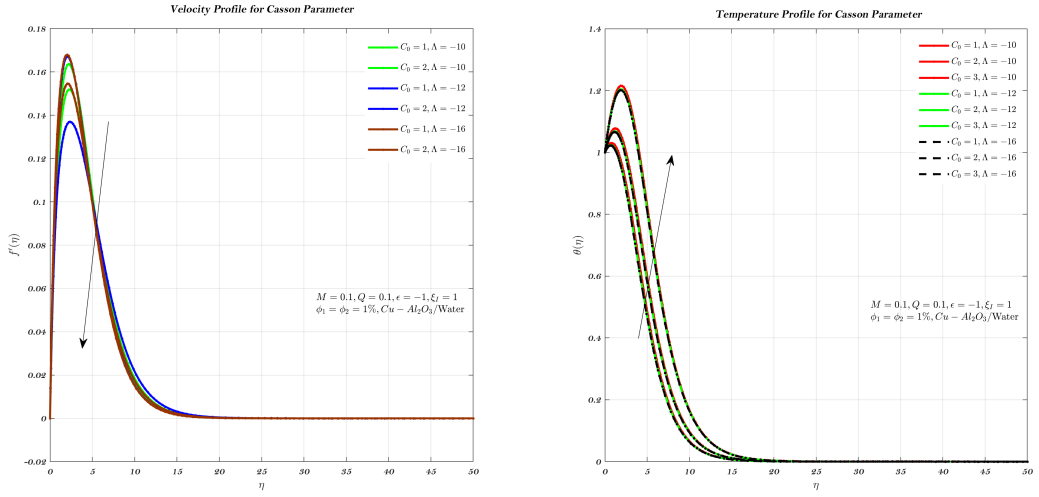

(a) Velocity profile. (b) Temperature profile.

Figure 7: Impact of Casson parameter.

which is vital in uses requiring effective thermal management. The Casson fluid model considerably disturbs the velocity and temperature profiles of the hybrid nanofluid. The flow percentage contracts as the Casson parameters increase, signifying more resistance to flow. Furthermore, the temperature diminishes with improved C_0 and more negative Λ, indicating enhanced heat transport. These discoveries are significant for manufacturing uses, mainly in systems that depend on effective heat dissipation and fluid flow regulation, including cooling systems in electronic procedures, automotive systems, and engineering uses. The outcomes climax the essential function of Casson parameters in increasing the efficacy of nano-fluids for thermal management and fluid flow claims.

5. Conclusions

This study employs a mathematical modeling approach to analyze the combined effects of magnetic fields, heat source/sink, mixed convection, and stagnation point flow on the behavior of a Casson hybrid nanofluid over a permeable stretching/shrinking surface. A computational technique is implemented to investigate how these key parameters influence the fluid dynamics and heat transfer characteristics of the hybrid nanofluid system. The research focuses on evaluating the intricate interactions between electromagnetic forces, thermal modulation, and convective transport phenomena in the boundary layer flow. Principal findings reveal significant modifications in flow patterns and thermal distributions due to the interplay of these physical factors. The study provides quantitative insights into how surface permeability and stretching/shrinking dynamics affect the system's overall performance. These results contribute to a deeper understanding of hybrid nanofluid behavior in complex flow configurations, with potential implications for thermal management

systems and industrial applications involving magneto-hydrodynamic flows:

- The velocity profile becomes progressively more pronounced and well-defined throughout the boundary layer region. This velocity enhancement occurs due to the combined effects of the fluid's non-Newtonian rheology and the electromagnetic body forces generated by the applied magnetic field. Simultaneously, the thermal boundary layer demonstrates an opposite response, with the temperature distribution showing a consistent decrease across the domain.

- The comparative analysis reveals that water demonstrates superior heat transfer performance compared to the $Cu - Al_2O_3/water$ hybrid nanofluid. Additionally, when evaluating $Al_2O_3/water$ nanofluid against the hybrid $Cu - Al_2O_3/water$ nanofluid, the former exhibits enhanced thermal transfer capabilities.

- Increasing the Casson parameter enhances the fluid's resistance to flow and deformation, reducing velocity, while decreasing it improves flow characteristics and increases velocity.

- At low values of Λ, opposing movements between the free stream and plate prevent definitive solutions. As ϕ_2 increases, the range for dual solutions narrows, the first solution shows velocity enhancement while the second shows reduction, with both solutions exhibiting temperature rise with increasing ϕ_2.

References

[1] Paul McElfresh, David Holcomb, and Daniel Ector. Application of nanofluid technology to improve recovery in oil and gas wells. In *SPE international oilfield nanotechnology conference and exhibition*. OnePetro, 2012.

[2] Kaufui V Wong and Omar De Leon. Applications of nanofluids: current and future. *Advances in mechanical engineering*, 2:519659, 2010.

[3] Ali Imran, Rizwan Akhtar, Zhu Zhiyu, Muhammad Shoaib, and Muhammad Asif Zahoor Raja. Heat transfer analysis of biological nanofluid flow through ductus efferentes. *AIP Advances*, 10(3):035029, 2020.

[4] WA Khan and I Pop. Boundary-layer flow of a nanofluid past a stretching sheet. *International journal of heat and mass transfer*, 53(11-12):2477–2483, 2010.

[5] Alin V Roşca and Ioan Pop. Flow and heat transfer over a vertical permeable stretching/shrinking sheet with a second order slip. *International Journal of Heat and Mass Transfer*, 60:355–364, 2013.

[6] H Zargartalebi, M Ghalambaz, A Noghrehabadi, and A Chamkha. Stagnation-point heat transfer of nanofluids toward stretching sheets with variable thermo-physical properties. *Advanced Powder Technology*, 26(3):819–829, 2015.

[7] Dhananjay Yadav, GS Agrawal, and Jinho Lee. Thermal instability in a rotating nanofluid layer: a revised model. *Ain Shams Engineering Journal*, 7(1):431–440, 2016.

[8] Shah Jahan, Hamzah Sakidin, Roslinda Nazar, and Ioan Pop. Flow and heat transfer past a permeable nonlinearly stretching/shrinking sheet in a nanofluid: A revised model with stability analysis. *Journal of Molecular Liquids*, 233:211–221, 2017.

[9] SA Mohammadein, K Raslan, MS Abdel-Wahed, and Elsayed M Abedel-Aal. Kkl-model of mhd cuo-nanofluid flow over a stagnation point stretching sheet with non-linear thermal radiation and suction/injection. *Results in Physics*, 10:194–199, 2018.

[10] Mohamed Abdelghany Elkotb, Aamir Hamid, M Riaz Khan, Muhammad Naveed Khan, and Ahmed M Galal. Thermal radiation and chemically reactive aspects of mixed convection flow using water base nanofluids: Tiwari and das model. *Waves in Random and Complex Media*, pages 1–31, 2021.

[11] Wasim Jamshed, SR Mishra, PK Pattnaik, Kottakkaran Sooppy Nisar, S Suriya Uma Devi, M Prakash, Faisal Shahzad, Majid Hussain, and V Vijayakumar. Features of entropy optimization on viscous second grade nanofluid streamed with thermal radiation: A tiwari and das model. *Case Studies in Thermal Engineering*, 27:101291, 2021.

[12] AV Kuznetsov and DA Nield. Natural convective boundary-layer flow of a nanofluid past a vertical plate. *International Journal of Thermal Sciences*, 49(2):243–247, 2010.

[13] AV Kuznetsov and DA Nield. Natural convective boundary-layer flow of a nanofluid past a vertical plate: A revised model. *International journal of thermal sciences*, 77:126–129, 2014.

[14] US Mahabaleshwar, KN Sneha, and Huang-Nan Huang. An effect of mhd and radiation on cnts-water based nanofluids due to a stretching sheet in a newtonian fluid. *Case Studies in Thermal Engineering*, 28:101462, 2021.

[15] AB Vishalakshi, US Mahabaleshwar, and Ioannis E Sarris. An mhd fluid flow over a porous stretching/shrinking sheet with slips and mass transpiration. *Micromachines*, 13(1):116, 2022.

[16] Furqan Jamil and Hafiz Muhammad Ali. Applications of hybrid nanofluids in different fields. In *Hybrid nanofluids for convection heat transfer*, pages 215–254. Elsevier, 2020.

[17] S Suriya Uma Devi and SP Anjali Devi. Numerical investigation of three-dimensional hybrid cu–al2o3/water nanofluid flow over a stretching sheet with effecting lorentz force subject to newtonian heating. *Canadian Journal of Physics*, 94(5):490–496, 2016.

[18] Mohammad Yousefi, Saeed Dinarvand, Mohammad Eftekhari Yazdi, and Ioan Pop. Stagnation-point flow of an aqueous titania-copper hybrid nanofluid toward a wavy cylinder. *International Journal of Numerical Methods for Heat & Fluid Flow*, 2018.

[19] Umer Farooq, Muhammad Idrees Afridi, Muhammad Qasim, and DC7513191 Lu. Transpiration and viscous dissipation effects on entropy generation in hybrid nanofluid flow over a nonlinear radially stretching disk. *Entropy*, 20(9):668, 2018.

[20] S Amala and B Mahanthesh. Hybrid nanofluid flow over a vertical rotating plate in the presence of hall current, nonlinear convection and heat absorption. *Journal of Nanofluids*, 7(6):1138–1148, 2018.

[21] Gabriela Huminic and Angel Huminic. Entropy generation of nanofluid and hybrid nanofluid flow in thermal systems: a review. *Journal of Molecular Liquids*, 302:112533,

2020.

[22] Iskandar Waini, Anuar Ishak, and Ioan Pop. Hybrid nanofluid flow towards a stagnation point on an exponentially stretching/shrinking vertical sheet with buoyancy effects. *International Journal of Numerical Methods for Heat & Fluid Flow*, 31(1):216–235, 2020.

[23] Nur Adilah Liyana Aladdin, Norfifah Bachok, and I Pop. Cu-al2o3/water hybrid nanofluid flow over a permeable moving surface in presence of hydromagnetic and suction effects. *Alexandria Engineering Journal*, 59(2):657–666, 2020.

[24] Najiyah Safwa Khashi'ie, Norihan Md Arifin, Ioan Pop, and Roslinda Nazar. Dual solutions of bioconvection hybrid nanofluid flow due to gyrotactic microorganisms towards a vertical plate. *Chinese Journal of Physics*, 72:461–474, 2021.

[25] Umair Khan, Aurang Zaib, Sakhinah Abu Bakar, Nepal Chandra Roy, and Anuar Ishak. Buoyancy effect on the stagnation point flow of a hybrid nanofluid toward a vertical plate in a saturated porous medium. *Case Studies in Thermal Engineering*, 27:101342, 2021.

[26] Vemula Rajesh, Mikhail A Sheremet, and Hakan F Öztop. Impact of hybrid nanofluids on mhd flow and heat transfer near a vertical plate with ramped wall temperature. *Case Studies in Thermal Engineering*, 28:101557, 2021.

[27] Meenakumari Ramamoorthy and Lakshminarayana Pallavarapu. Second order slip flow of a conducting jeffrey nanofluid in an inclined asymmetric porous conduit with heat and mass transfer. *Multidiscipline Modeling in Materials and Structures*, (ahead-of-print), 2022.

[28] Ali Raza, Umair Khan, Zehba Raizah, Sayed M Eldin, Abeer M Alotaibi, Samia Elattar, and Ahmed M Abed. Numerical and computational analysis of magnetohydrodynamics over an inclined plate induced by nanofluid with newtonian heating via fractional approach. *Symmetry*, 14(11):2412, 2022.

[29] Prakash Jayavel, Dharmendra Tripathi, O Anwar Bég, Abhishek Kumar Tiwari, and Rakesh Kumar. Thermo-electrokinetic rotating non-newtonian hybrid nanofluid flow from an accelerating vertical surface. *Heat Transfer*, 51(2):1746–1777, 2022.

[30] Nurul Amira Zainal, Roslinda Nazar, Kohilavani Naganthran, and Ioan Pop. Mhd mixed convection stagnation point flow of a hybrid nanofluid past a vertical flat plate with convective boundary condition. *Chinese Journal of Physics*, 66:630–644, 2020.

[31] P Gokulavani, S Muthukumar, S Sureshkumar, M Muthtamilselvan, and Qasem M Al-Mdallal. Computational analysis of mhd flow in a porous open chamber filled with hybrid nanofluid and vertical heat sources. *Journal of Thermal Analysis and Calorimetry*, pages 1–16, 2025.

[32] Nurul Amira Zainal, Dg Marina Mokhtar, Iskandar Waini, Haris Alam Zuberi, Roslinda Nazar, and Ioan Pop. Mixed convection of couple stress hybrid nanofluid past a vertical shrinking plate. *Journal of Thermal Analysis and Calorimetry*, pages 1–9, 2025.

[33] Mageswari Manimaran, Mohd Nurazzi Norizan, Mohamad Haafiz Mohamad Kassim, Mohd Ridhwan Adam, Norli Abdullah, and Mohd Nor Faiz Norrrahim. Critical review on the stability and thermal conductivity of water-based hybrid nanofluids for heat

transfer applications. *RSC advances*, 15(18):14088–14125, 2025.

[34] S Hussain, SM Atif, M Sagheer, and MA Manzoor. Mhd carreau nanofluid with arrhenius activation energy in a porous medium. *Scientia Iranica*, 29(6):3591–3602, 2022.

[35] Rahila Naz, Muhamamd Sohail, Memoona Bibi, and Maryiam Javed. Numerical treatment of magneto hydrodynamic carreau liquid with heat and mass transport containing gyrotactic microorganisms. *Scientia Iranica*, 30(6):2223–2234, 2023.

[36] MH Saeed, SM Alduwaib, and DJ Al-den. Investigation of structural, photoluminescence and self-cleaning properties of thin layers of go-zno and go, go-ag and composite bilayer of go-zno/go-ag prepared by spray pyrolysis method. *Scientia Iranica*, 31(12):958–966, 2024.

[37] JK Madhukesh, GK Ramesh, and YB Revadakundi. Thermal transport analysis of ternary hybrid nanofluid flow over a vertical cylinder with thermal radiation and chemical reaction. *Thermal Advances*, 3:100040, 2025.

[38] Maddina Dinesh Kumar, Gurram Dharmaiah, Se-Jin Yook, CSK Raju, and Nehad Ali Shah. Deep learning approach for predicting heat transfer in water-based hybrid nanofluid thin film flow and optimization via response surface methodology. *Case Studies in Thermal Engineering*, 68:105930, 2025.

[39] Ahmed M Galal, SR Mishra, Rupa Baithalu, Mohamed Kallel, Subhajit Panda, Ali J Chamkha, Rifaqat Ali, and SR Afshar. Three-dimensional flow of nanofluid through a vertical channel considering kkl model: Hydrothermal analysis via response surface methodology. *Journal of the Taiwan Institute of Chemical Engineers*, 168:105931, 2025.

[40] P Francis, P Sambath, S Noeiaghdam, U Fernandez-Gamiz, and S Dinarvand. Computational analysis of bioconvective mhd hybrid nanofluid flow of non-newtonian fluid over cone/plate: A study based on the cattaneo-christov heat and mass flux model. *Engineering Science and Technology, an International Journal*, 63:101970, 2025.

[41] Aneela Bibi, Hang Xu, Qiang Sun, Ioan Pop, and Qingkai Zhao. Free convection of a hybrid nanofluid past a vertical plate embedded in a porous medium with anisotropic permeability. *International Journal of Numerical Methods for Heat & Fluid Flow*, 2020.

[42] Muhammad Nadeem, Ahmed Elmoasry, Imran Siddique, Fahd Jarad, Rana Muhammad Zulqarnain, Jawdat Alebraheem, and Naseer S Elazab. Study of triangular fuzzy hybrid nanofluids on the natural convection flow and heat transfer between two vertical plates. *Computational Intelligence and Neuroscience*, 2021, 2021.

[43] Nur Syahirah Wahid, Norihan Md Arifin, Najiyah Safwa Khashi'ie, Ioan Pop, Norfifah Bachok, and Mohd Ezad Hafidz Hafidzuddin. Mhd mixed convection flow of a hybrid nanofluid past a permeable vertical flat plate with thermal radiation effect. *Alexandria Engineering Journal*, 61(4):3323–3333, 2022.

[44] Ali Rehman, Dolat Khan, Ibrahim Mahariq, Mohamed Abdelghany Elkotb, and Thanaa Elnaqeeb. Viscous dissipation effects on time-dependent mhd casson nanofluid over stretching surface: A hybrid nanofluid study. *Journal of Molecular Liquids*, 408:125370, 2024.

[45] Adrian Bejan. *Convection heat transfer*. John wiley & sons, 2013.

[46] Ali J Chamkha and AM Aly. Mhd free convection flow of a nanofluid past a vertical plate in the presence of heat generation or absorption effects. *Chemical Engineering Communications*, 198(3):425–441, 2010.

[47] Wubshet Ibrahim and Bandari Shanker. Boundary-layer flow and heat transfer of nanofluid over a vertical plate with convective surface boundary condition. *Journal of fluids engineering*, 134(8), 2012.

[48] Wubshet Ibrahim and OD Makinde. The effect of double stratification on boundary-layer flow and heat transfer of nanofluid over a vertical plate. *Computers & Fluids*, 86:433–441, 2013.

[49] Mohammadreza Nademi Rostami, Saeed Dinarvand, and Ioan Pop. Dual solutions for mixed convective stagnation-point flow of an aqueous silica–alumina hybrid nanofluid. *Chinese journal of physics*, 56(5):2465–2478, 2018.

[50] Hakan F Oztop and Eiyad Abu-Nada. Numerical study of natural convection in partially heated rectangular enclosures filled with nanofluids. *International journal of heat and fluid flow*, 29(5):1326–1336, 2008.

[51] M Turkyilmazoglu. Dual and triple solutions for mhd slip flow of non-newtonian fluid over a shrinking surface. *Computers & Fluids*, 70:53–58, 2012.

[52] Mohsen Sheikholeslami Kandelousi. Kkl correlation for simulation of nanofluid flow and heat transfer in a permeable channel. *Physics Letters A*, 378(45):3331–3339, 2014.

[53] Mohsen Sheikholeslami, Shirley Abelman, and Davood Domiri Ganji. Numerical simulation of mhd nanofluid flow and heat transfer considering viscous dissipation. *International Journal of Heat and Mass Transfer*, 79:212–222, 2014.

[54] Mohsen Sheikholeslami and Shirley Abelman. Two-phase simulation of nanofluid flow and heat transfer in an annulus in the presence of an axial magnetic field. *IEEE Transactions on Nanotechnology*, 14(3):561–569, 2015.

[55] Mustafa Turkyilmazoglu. An analytical treatment for the exact solutions of mhd flow and heat over two–three dimensional deforming bodies. *International Journal of Heat and Mass Transfer*, 90:781–789, 2015.

[56] Mustafa Turkyilmazoglu. A note on the correspondence between certain nanofluid flows and standard fluid flows. *Journal of Heat Transfer*, 137(2), 2015.

[57] Mohsen Sheikholeslami and Rahmat Ellahi. Three dimensional mesoscopic simulation of magnetic field effect on natural convection of nanofluid. *International Journal of Heat and Mass Transfer*, 89:799–808, 2015.

[58] Anuar Jamaludin, Kohilavani Naganthran, Roslinda Nazar, and Ioan Pop. Thermal radiation and mhd effects in the mixed convection flow of fe3o4–water ferrofluid towards a nonlinearly moving surface. *Processes*, 8(1):95, 2020.

[59] Muhammad Shoaib Bhutta, Tang Xuebang, Shakeel Akram, Chen Yidong, Xiancheng Ren, Muhammad Fasehullah, Ghulam Rasool, and Muhammad Tariq Nazir. Development of novel hybrid 2d-3d graphene oxide diamond micro composite polyimide films to ameliorate electrical & thermal conduction. *Journal of Industrial and Engineering Chemistry*, 114:108–114, 2022.

[60] Yuzhen Gao and Choon Kit Chan. Numerical simulation of dense-phase pneumatic

conveying in vertical pipe for gasifier. *Polish Journal of Chemical Technology*, 25(3), 2023.

[61] Yuzhen Gao and Choon Kit Chan. Cfd-dem simulation of raceway size and mechanical characteristics of industrial scale blast furnace. *Polish Journal of Chemical Technology*, 25(3):71–78, 2023.

[62] Manishaa Sri Mahendran, Ling Shing Wong, Anto Cordelia Tanislaus Antony Dhanapal, and Sinouvassane Djearamane. The effect of titanium dioxide nanoparticles on haematococcus pluvialis biomass concentration. 2023.

[63] Mohankumar Palaniswamy. Medical equipment engineering in industrial revolution. IET.

[64] Zulqurnain Sabir, Ali Imran, Muhammad Umar, Muhammad Zeb, Muhammad Shoaib, and Muhammad Asif Zahoor Raja. A numerical approach for 2-d sutterby fluid-flow bounded at a stagnation point with an inclined magnetic field and thermal radiation impacts. *Thermal Science*, 25(3 Part A):1975–1987, 2021.

[65] Abdeldjebbar Tounsi, Zakaria Belabed, Fatima Bounouara, Mohammed Balubaid, SR Mahmoud, Abdelmoumen Anis Bousahla, and Abdelouahed Tounsi. A finite element approach for forced dynamical responses of porous fg nanocomposite beams resting on viscoelastic foundations. *International Journal of Structural Stability and Dynamics*, page 2650078, 2024.

[66] Zakaria Belabed, Abdeldjebbar Tounsi, Abdelmoumen Anis Bousahla, Abdelouahed Tounsi, and Murat Yaylacı. Accurate free and forced vibration behavior prediction of functionally graded sandwich beams with variable cross-section: a finite element assessment. *Mechanics Based Design of Structures and Machines*, 52(11):9144–9177, 2024.

[67] Zakaria Belabed, Abdelmoumen Anis Bousahla, and Abdelouahed Tounsi. Vibrational and elastic stability responses of functionally graded carbon nanotube reinforced nanocomposite beams via a new quasi-3d finite element model. *Computers and Concrete*, 34(5):625–648, 2024.

[68] Zakaria Belabed, Abdeldjebbar Tounsi, Abdelmoumen Anis Bousahla, Abdelouahed Tounsi, Khaled Mohamed Khedher, and Mohamed Abdelaziz Salem. Mechanical behavior analysis of fg-cntrc porous beams resting on winkler and pasternak elastic foundations: a finite element approach. *Computers and Concrete*, 34(4):447–476, 2024.

[69] Zakaria Belabed, Abdeldjebbar Tounsi, Abdelmoumen Anis Bousahla, Abdelouahed Tounsi, Mohamed Bourada, and Mohammed A Al-Osta. Free vibration analysis of bi-directional functionally graded beams using a simple and efficient finite element model. *Structural Engineering and Mechanics, An Int'l Journal*, 90(3):233–252, 2024.

[70] Zakaria Belabed, Abdelouahed Tounsi, Mohammed A Al-Osta, Abdeldjebbar Tounsi, and Hoang-Le Minh. On the elastic stability and free vibration responses of functionally graded porous beams resting on winkler-pasternak foundations via finite element computation. *Geomechanics & engineering*, 36(2):183–204, 2024.

[71] Hakim Bentrar, Sidi Mohammed Chorfi, Sid Ahmed Belalia, Abdelouahed Tounsi, Mofareh Hassan Ghazwani, and Ali Alnujaie. Effect of porosity distribution on free

vibration of functionally graded sandwich plate using the p-version of the finite element method. *Structural engineering and mechanics: An international journal*, 88(6):551–567, 2023.

[72] Varun Katiyar, Ankit Gupta, and Abdelouahed Tounsi. Microstructural/geometric imperfection sensitivity on the vibration response of geometrically discontinuous bi-directional functionally graded plates (2dfgps) with partial supports by using fem. *Steel and Composite Structures*, pages 621–640, 2022.

[73] Muhammad Azam, Nadeem Abbas, K Ganesh Kumar, and Samad Wali. Transient bioconvection and activation energy impacts on casson nanofluid with gyrotactic microorganisms and nonlinear radiation. *Waves in Random and Complex Media*, pages 1–20, 2022.

[74] Manjappa Archana, Mundalamane Manjappa Praveena, Kondlahalli Ganesh Kumar, Sabir Ali Shehzad, and Manzoor Ahmad. Unsteady squeezed casson nanofluid flow by considering the slip condition and time-dependent magnetic field. *Heat transfer*, 49(8):4907–4922, 2020.

[75] M Gnaneswara Reddy, P Vijayakumari, MVVNL Sudharani, and K Ganesh Kumar. Quadratic convective heat transport of casson nanoliquid over a contract cylinder: an unsteady case. *BioNanoScience*, 10(1):344–350, 2020.

[76] HJ Lokesh, BJ Gireesha, and K Ganesh Kumar. Characterization of chemical reaction on magnetohydrodynamics flow and nonlinear radiative heat transfer of casson nanoparticles over an exponentially sheet. *Journal of Nanofluids*, 8(6):1260–1266, 2019.

[77] BS Dhruvathara, Padmavathi R, K Ganesh Kumar, Waseem Sharaf Saeed, and Aqeel Afzal. Emhd flow and convective heat transfer over a prescribed surface temperature (pst) and prescribed heat flux (phf) heating condition. *Numerical Heat Transfer, Part A: Applications*, 86(2):201–214, 2025.

[78] R Vinutha et al. Theoretical analysis of effect of mhd, couple stress and slip velocity on squeeze film lubrication of rough triangular plates. *International Journal of Thermofluids*, 24:100882, 2024.

[79] K Ganesh Kumar, DG Prakasha, MM Praveen, M Gnaneswara Reddy, and KR Vasanth. Physical characteristics of variable thermal conductivity and mhd flow across a continually stretched sheet. *Proceedings of the Institution of Mechanical Engineers, Part N: Journal of Nanomaterials, Nanoengineering and Nanosystems*, page 23977914241259087, 2024.

[80] Lal Sing Naik, DG Prakasha, MVVNL Sudharani, and K Ganesh Kumar. Effects of ohmic and activation energy on the physical characteristics of mhd flow and variable heat transfer to a different fluids. *International Journal of Modern Physics B*, 38(18):2450241, 2024.

[81] Ali J Chamkha and Eiyad Abu-Nada. Mixed convection flow in single-and double-lid driven square cavities filled with water–al2o3 nanofluid: Effect of viscosity models. *European Journal of Mechanics-B/Fluids*, 36:82–96, 2012.

[82] Mikhail A Sheremet, Ioan Pop, and OJIJOH Mahian. Natural convection in an inclined cavity with time-periodic temperature boundary conditions using nanofluids:

application in solar collectors. *International Journal of Heat and Mass Transfer*, 116:751–761, 2018.

[83] Mikhail Alexandrovich Sheremet, T Grosan, and Ioan Pop. Free convection in a square cavity filled with a porous medium saturated by nanofluid using tiwari and das' nanofluid model. *Transport in Porous Media*, 106(3):595–610, 2015.

[84] Mohammad Hemmat Esfe, Mohammad Akbari, Davood Semiromi Toghraie, Arash Karimipour, and Masoud Afrand. Effect of nanofluid variable properties on mixed convection flow and heat transfer in an inclined two-sided lid-driven cavity with sinusoidal heating on sidewalls. *Heat Transfer Research*, 45(5), 2014.

[85] Muneer A Ismael, Eiyad Abu-Nada, and Ali J Chamkha. Mixed convection in a square cavity filled with cuo-water nanofluid heated by corner heater. *International Journal of Mechanical Sciences*, 133:42–50, 2017.

[86] Qiang Sun and Ioan Pop. Free convection in a triangle cavity filled with a porous medium saturated with nanofluids with flush mounted heater on the wall. *International journal of thermal sciences*, 50(11):2141–2153, 2011.

[87] MK Das and RK Tiwari. Transient mixed convection in a two-sided lid-driven differentially heated square cavity utilizing nanofluids. *Proceedings of the Institution of Mechanical Engineers, Part N: Journal of Nanoengineering and Nanosystems*, 223(2):63–74, 2009.

[88] Farooq Ahmad, H Waqas, Hela Ayed, Sajjad Hussain, S Farooq, SA Khan, and A Othman Almatroud. Numerical treatment with lobatto-iiia scheme magneto-thermo-natural convection flow of casson nanofluid (mos2- cu/sa) configured by a stretching cylinder in porous medium with multiple slips. *Case Studies in Thermal Engineering*, 26:101132, 2021.

[89] Najiyah Safwa Khashi'ie, Norihan M Arifin, Ioan Pop, Roslinda Nazar, and Ezad Hafidz Hafidzuddin. A new similarity solution with stability analysis for the three-dimensional boundary layer of hybrid nanofluids. *International Journal of Numerical Methods for Heat & Fluid Flow*, 2020.

[90] Anuar Ishak, Roslinda Nazar, and Ioan Pop. The effects of transpiration on the flow and heat transfer over a moving permeable surface in a parallel stream. *Chemical Engineering Journal*, 148(1):63–67, 2009.